

# DIP: Efficient Large Multimodal Model Training with Dynamic Interleaved Pipeline

Zhenliang Xue

Institute of Parallel and Distributed  
Systems  
Shanghai Jiao Tong University  
Shanghai, China  
xuezhengliang@sjtu.edu.cn

Hanpeng Hu

StepFun  
Shanghai, China  
haanpeng@outlook.com

Xing Chen

StepFun  
Shanghai, China  
xchen382@asu.edu

Yimin Jiang

StepFun  
Shanghai, China  
jymthu@gmail.com

Yixin Song

Institute of Parallel and Distributed  
Systems  
Shanghai Jiao Tong University  
Shanghai, China  
yixinsong@sjtu.edu.cn

Zeyu Mi

Institute of Parallel and Distributed  
Systems  
Shanghai Jiao Tong University  
Shanghai, China  
yzmizeyu@sjtu.edu.cn

Yibo Zhu

StepFun  
Shanghai, China  
zhuyibo@stepfun.com

Daxin Jiang

StepFun  
Shanghai, China  
djiang@stepfun.com

Yubin Xia

Institute of Parallel and Distributed  
Systems  
Shanghai Jiao Tong University  
Shanghai, China  
xiayubin@sjtu.edu.cn

Haibo Chen

Institute of Parallel and Distributed  
Systems  
Shanghai Jiao Tong University  
Shanghai, China  
haibo chen@sjtu.edu.cn

## Abstract

Large multimodal models (LMMs) have demonstrated excellent capabilities in both understanding and generation tasks with various modalities. While these models can accept flexible combinations of input data, their training efficiency suffers from two major issues: pipeline stage imbalance caused by heterogeneous model architectures, and training data dynamicity stemming from the diversity of multimodal data.

In this paper, we present DIP, a dynamic and modality-aware pipeline scheduling framework designed for LMM training. DIP tackles the challenge of *dynamic imbalance* via two key techniques: (1) separating computations of different modalities into dedicated *pipeline segments* to balance workloads within a continuous set of stages; (2) dynamically

splitting input data into finer-grained, modality-specific *sub-microbatches* to balance workloads across these segments. By asynchronously generating pipeline schedules on idle CPU resources during training, DIP dynamically tailors stage executions to each input batch without stalling the training process. We validate DIP on a diverse set of five LMMs, ranging from 12B to 94B parameters and including vision-language and diffusion models. Experimental results show that our system achieves up to 97.3% higher throughput compared to state-of-the-art systems, demonstrating strong adaptability to fluctuating multimodal training workloads.

**CCS Concepts:** • Computing methodologies → Distributed computing methodologies; Modeling and simulation.

**Keywords:** Large-Scale Training; Large Multimodal Models; Distributed Systems; Simulation

## ACM Reference Format:

Zhenliang Xue, Hanpeng Hu, Xing Chen, Yimin Jiang, Yixin Song, Zeyu Mi, Yibo Zhu, Daxin Jiang, Yubin Xia, and Haibo Chen. 2026. DIP: Efficient Large Multimodal Model Training with Dynamic Interleaved Pipeline. In *Proceedings of the 31st ACM International Conference on Architectural Support for Programming Languages*



This work is licensed under a Creative Commons Attribution 4.0 International License.

ASPLOS '26, Pittsburgh, PA, USA

© 2026 Copyright held by the owner/author(s).

ACM ISBN 979-8-4007-2359-9/2026/03

<https://doi.org/10.1145/3779212.3790154>

and Operating Systems, Volume 2 (ASPLOS '26), March 22–26, 2026, Pittsburgh, PA, USA. ACM, New York, NY, USA, 15 pages. <https://doi.org/10.1145/3779212.3790154>

## 1 Introduction

Transformer-based models [11, 17, 44, 51] have demonstrated remarkable capabilities in multimodal understanding, reasoning, and generation, establishing themselves as foundational architectures for next-generation large multimodal models (LMMs) [2, 10, 17, 18, 31, 32]. Modern LMMs integrate multiple *modality modules*, including encoders, decoders, and backbone models connected via modality adapters. This architectural design enables flexible and seamless processing of interleaved multimodal data (e.g., text, images, video), thereby supporting diverse task paradigms such as multimodal document understanding [8] and multi-turn dialogs [33].

However, this architectural flexibility introduces significant challenges in training due to irregular and fluctuating execution latencies across different modality modules and data batches, leading to a unique problem of *dynamic imbalance*. This challenge stems from two interrelated factors:

**Pipeline Stage Imbalance:** LMMs exhibit architectural heterogeneity arising from diverse modality modules with distinct parameter shapes and operator types (e.g., attention, GEMM, convolution). These differences create skewed computational workloads and varying memory access patterns, complicating the partitioning of model execution into balanced pipeline stages. Even with exhaustive enumeration of all possible layer splits, the “optimal” partitioning still incurs a 22.8% pipeline bubble overhead for a 37B-parameter LMM (§2.3). This inefficiency is primarily due to the significant discrepancy between heterogeneous layers, which prevents perfectly balanced pipeline stage partitioning.

**Training Data Dynamicity:** The inherent architectural heterogeneity is further exacerbated by the diversity of multimodal training data, which comprises large-scale datasets with highly variable modality distributions across batches. Although data packing techniques [24, 48] aim to produce more balanced batches, computational imbalance persists. In our experiments, the largest data sample incurs 4.15× greater computational load than the smallest (§2.2). Such disparities cause substantial workload fluctuations between batches.

The combination of pipeline stage imbalance and training data dynamicity results in a significant performance bottleneck. Our experiments show that this dynamic imbalance can inflate training overhead by up to 40.3% for the 37B LMM (§2.3). This performance degradation renders the conventional approach of using a single, static pipeline schedule (e.g., Megatron-LM’s 1F1B) impractical and inefficient for the dynamic nature of LMMs. Similarly, training systems for multimodal models such as Spindle [47] and Optimus [15] rely on static pipeline schedules tailored for a fixed set of tasks. Their training plans are determined before training start, overlooking the dynamic nature of multimodal data

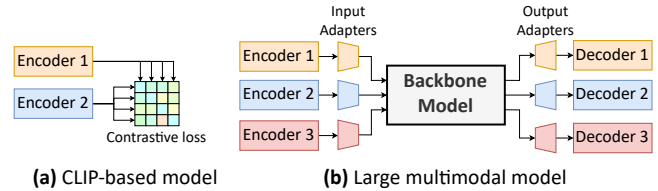


Figure 1. Comparison between CLIP-based models and LMMs.

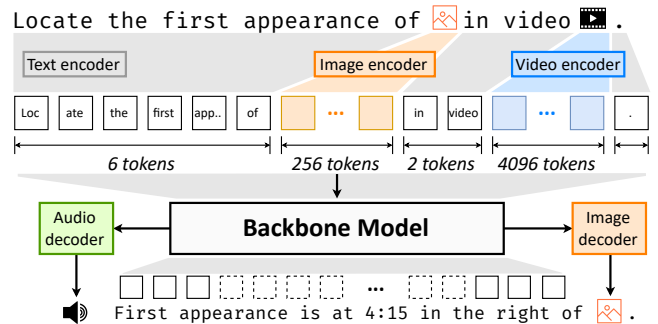


Figure 2. An example of LMM that uses a large language model as the backbone. The user prompt consists of an image and a video clip, and is converted into tokens by corresponding modality encoders, which are further processed by the backbone model to produce the response in multimodal text or speech audio.

and resulting in suboptimal pipeline performance. Existing approaches [24, 48, 54] designed for dynamic text sequence lengths are also insufficient. They primarily address workload variations that affect all layers of a unimodal LLM uniformly. However, they cannot resolve the fundamental intermodality imbalance in LMMs, where a change in one modality (e.g., more images) can drastically overload a specific module while leaving others underutilized.

To address these challenges, we propose DIP, a dynamic and modality-aware scheduling framework designed to optimize pipeline parallelism for LMMs. DIP is built upon two key insights that identify the root causes of pipeline inefficiency. First, co-locating computations from different modality modules within the same pipeline execution pass is inherently inefficient due to their disparate computational costs (Fig. 5a). We define a *pipeline segment* as a complete forward or backward pass of computations across all pipeline stages. To eliminate this *intra-segment imbalance*, DIP enforces separated partitioning, dedicating distinct pipeline segments to each modality (Fig. 5b). This isolation prevents slow modalities from bottlenecking faster ones. Second, even after separation, workload imbalances persist between these modality-specific segments. To resolve this *inter-segment imbalance*, DIP further dynamically splits data into smaller, modality-specific *sub-microbatches* (Fig. 5c). This modality-aware partitioning approach allows latencies of different modality segments to be more closely matched, resulting in finer-grained load balancing between these segments.

Meanwhile, in contrast to conventional systems that rely on static or pre-computed schedules, DIP employs asynchronous schedule generation. It generates a custom pipeline schedule for each data batch on-the-fly, seamlessly adapting to the fluctuating computational demands of multimodal data. To avoid stalling training, DIP generates schedules using idle CPU cores in parallel with the main GPU training workers, effectively hiding search latency. To identify high-quality schedules within the tight time constraints of a training iteration (typically 10–60 seconds), DIP decomposes the complex search problem into three simpler subproblems, each with a tailored heuristic to reduce search space. DIP parallelizes the search loop over hundreds of CPU cores, shortening the search time and harnessing idle CPUs.

We implement DIP on top of Megatron-LM, the state-of-the-art distributed training framework for transformer-based large language models. In addition to the scheduling algorithms, we develop a training simulator for fast and accurate prediction of pipeline stage latency and memory consumption. We also enhance Megatron-LM with a reconfigurable pipeline mechanism to support dynamic pipeline schedule deployment. We validate DIP on a diverse set of five LMMs, ranging from 12B to 94B parameters and including vision-language models and diffusion models. Experimental results demonstrate that DIP achieves up to 97.3% higher training performance compared to baseline systems. Moreover, DIP exhibits excellent adaptability to the dynamic workloads of LMM training, maintaining near-optimal hardware utilization throughout the training process.

In summary, this paper makes the following contributions:

- We identify and characterize the problem of dynamic imbalance in LMM training, a challenge arising from the interplay between pipeline stage imbalance and training data dynamicity.
- We propose DIP, a novel scheduling framework that employs asynchronous schedule generation, modality-aware partitioning, and a decomposed search algorithm to dynamically adapt to varying workloads.
- We evaluate DIP against three state-of-the-art training systems across five LMM models up to 94B, demonstrating improvements of up to 97.3% in training efficiency.

## 2 Dynamic Imbalance Characterization

### 2.1 Large Multimodal Models

Multimodal models have long sought to bridge heterogeneous modalities by learning unified semantic representations [40]. Early CLIP-based multimodal models [37] pioneered the dual-encoder architecture (e.g., ViT for images, BERT for text) and employed contrastive loss [6] to align cross-modal embeddings in shared semantic spaces.

The advent of large multimodal models (LMM) marks a paradigm shift that extends beyond representation alignment

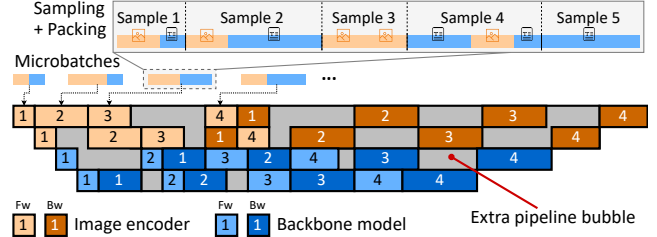


Figure 3. Illustration of the impact of dynamic imbalance.

to encompass multimodal generation capabilities. This evolution is driven by the integration of large-scale transformer-based architectures, such as large language models (LLMs), vision transformers (ViT), and diffusion transformers (DiT). LMMs integrate encoders with the backbone model using modality adapters, as illustrated in Fig. 1. The backbone model subsequently generates output representations either through autoregressive processes or diffusion mechanisms. These representations are then converted into human-perceivable formats, including text, audio, and images, via specialized modality decoders. The scalable and generative architecture of LMM significantly broadens the spectrum of supported tasks compared to CLIP-based models. For instance, in an LMM (Fig. 2), users can interleave text, images, and video within a single query and iteratively refine their queries by appending follow-up questions to create multi-turn dialogs [10, 20, 33]. The LMM can respond in text or speech [18], and generate images using diffusion modules [27, 31, 35].

**LMM Training.** Large transformer-based models are typically trained with 3D distributed schemes such as data parallelism (DP), pipeline parallelism (PP), and tensor parallelism (TP) [39]. Pipeline parallelism partitions model layers into multiple *model chunks* placed on different machines (i.e., pipeline ranks). Each model chunk can perform both forward and backward stage computations. Data batches are split into smaller microbatches and passed between pipeline stages with point-to-point (P2P) communications.

### 2.2 Sources of Dynamic Imbalance

Due to the heterogeneity of multimodal model architectures and the diversity of training data, the training process for LMMs differs significantly from that for unimodal models in *pipeline stage imbalance* and *training data dynamicity*.

**Pipeline Stage Imbalance.** Optimal pipeline efficiency requires balanced stage partitioning to minimize bubbles, yet inherent computational disparities between modality modules introduce fundamental challenges. Consider a 37B VLM comprising a 5B ViT encoder (64 layers) and 32B language model (64 layers) on H800 GPUs, processing a batch with 8 images and 8192 text tokens. Each ViT layer processes the images in 6.75ms (forward+backward), while each LM

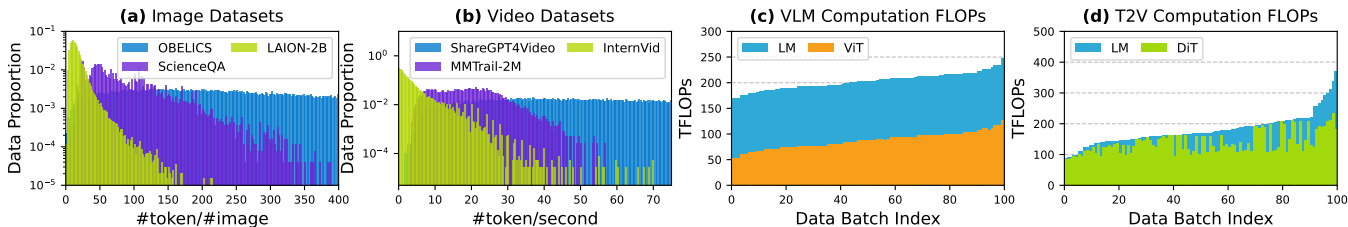


**Figure 4.** (a–b) Token distribution per image in OBELICS [25], LAION-2B [38], and ScienceQA [30] datasets, and token distribution per second in ShareGPT4Video [4], InternVid [46], and MMTrail-2M [7] video datasets. The Y-axis shows normalized data proportions. (c–d) Computational requirements for VLM 12B (VLM-S in Table 3) and T2V 13B (T2V-S in Table 3) models across 100 packed data batches. Batches (X-axis) are sorted by ascending computational cost, with floating-point operations (Y-axis) measured in teraFLOPs (TFLOPs).

layer requires 10.5ms for the tokens. The optimal partitioning scheme produced by exhaustive search across 16 pipeline stages yields stage latencies between 63ms and 73.5ms (i.e., 16.7% variation). With 64 microbatches and Megatron-LM’s 1F1B pipeline schedule, this imbalance introduces 22.8% additional pipeline bubbles, demonstrating the inherent difficulty in achieving perfectly balanced partitioning.

**Training Data Dynamicity.** This challenge is further compounded by the dynamic heterogeneity in multimodal training data, where the variability across batches from different modalities induces fluctuating computational demands. Multimodal data originates from diverse sources including: image-description pairs [3, 38], video with captions [4, 7, 46, 49], and interleaved image-text content [25, 58]. Data samples typically comprise images/videos with descriptive texts, exhibiting significant *cross-dataset variation* in modality data ratios (Fig. 4a–b). For instance, the LAION-2B [38] dataset consists of images paired with short captions, with a small text-image ratio (16.4 tokens/image), while the OBELICS [25] dataset contains full-length multimodal documents with highly variable ratios (0.4 to 3115 tokens/image).

This variation further induces *cross-batch imbalance* during data packing. Typically, data samples are packed into larger batches to enhance computation efficiency [24, 48]. In vision-language models (VLMs), both images and texts are tokenized (e.g., one image into 169 patch tokens) and then greedily packed up to the model’s context length (e.g., 8192 tokens) to form a microbatch. Similarly, for text-to-video (T2V) diffusion models, video clips with similar durations and aspect ratios are often grouped for batch processing [31, 35]. However, data packing fails to ensure balanced workloads across multiple modalities due to their divergent distributions (Fig. 4c–d). For instance, consider two microbatches with same 8192-token capacity: the first contains 10 images (i.e., 1690 patch tokens) accompanied by 6502 text tokens, whereas the second consists of only a single image and 8023 text tokens. These two microbatches impose disparate computational demands: the FLOPs required for the image pipeline stages in the first microbatch are 10× higher than those in the second. This discrepancy leads to imbalanced

**Table 1.** Training performance of 7B models on 8 GPUs (TP=2, PP=4). “PFLOPs” denotes the floating-point operations per iteration in petaFLOPs, which is controlled to a fixed value for fair comparison. “MFU” refers to model FLOPs utilization.

Model Setup	Time (s)	PFLOPs	MFU
LM 7B	4.068	12.8	0.400
ViT 2B + LM 5B (static data)	4.567	12.7	0.351
ViT 2B + LM 5B (dynamic data)	6.789	12.8	0.239

pipeline stages across microbatches (Fig. 3). Furthermore, for a T2V model comprising a 7B LM and a 5B DiT, the most computationally intensive batch (data batch index 100 in Fig. 4d) imposes a 4.15× greater computational load than the smallest batch (data batch index 1), even after data packing.

### 2.3 Negative Impact on Pipeline Parallelism

The combination of pipeline stage imbalance and training data dynamicity leads to the *dynamic imbalance* problem. As depicted in Fig. 3, this issue introduces significant pipeline bubbles in Megatron-LM’s 1F1B pipeline schedule, and severely degrades training throughput.

To quantify this impact, we compare two model setups with the same number of parameters: a unimodal LM (7B) and a vision-language model (ViT 2B + LM 5B). Under identical 1F1B pipeline configurations (using balanced parameter partitioning and fixed computational budgets), the VLM incurs a 12.5% overhead on static data due to stage imbalance. With real-world dynamic data, this overhead escalates to 40.3%, as shown in Table 1.

**Impact on Pipeline Design.** Such performance degradation renders the fixed pipeline schedules used in unimodal LLMs impractical. Since each iteration processes a distinct data batch, the optimal pipeline schedule changes dynamically.

Precomputation of pipeline schedules is also infeasible. The number of possible input combinations grows exponentially in two dimensions: the number of modalities and the number of microbatches. In our experimental setup, each microbatch can contain up to 48 images (§7.1), leading to

$49^{64} \approx 1.5e108$  distinct input configurations for 64 microbatches. This makes it impossible to exhaustively precompute optimal schedules for all scenarios. Although precomputing over a subset of inputs could reduce overhead, selecting a representative subset from this enormous space is highly challenging, and fails to generalize to unseen inputs.

Several prior works have addressed the issue of dynamicity in text sequence lengths, by improving data packing strategies to reduce discrepancies between microbatches [48], or adaptively reordering microbatches to minimize bubbles caused by irregular inputs [24, 54]. However, these methods are inadequate for solving dynamic imbalance in multimodal training, as they overlook the heterogeneity among modality modules. Unlike in unimodal LLMs, where sequence length variations affect all layers uniformly, multimodal microbatches affect modality-specific modules differently. For example, increasing the number of images substantially raises computational demands on image encoders, while barely affecting the language model backbone. This inter-modality imbalance makes data-centric approaches designed for unimodal models ineffective for LMM training.

### 3 Approach Overview

To address the challenges of pipeline stage imbalance and training data dynamicity, we introduce Dynamic Interleaved Pipeline (DIP), a dynamic and modality-aware scheduling framework designed to optimize pipeline parallelism for LMMs. DIP is built on three key design principles: asynchronous schedule generation to hide search latency, modality-aware partitioning to mitigate imbalance at its source, and decomposed search algorithm to find high-quality pipeline schedules efficiently.

#### 3.1 Design Principles

**Asynchronous Schedule Generation.** In contrast to conventional approaches that rely on static or pre-computed schedules, DIP adopts an online, asynchronous strategy, in order to handle the dynamic nature of LMM data. For each upcoming data batch, it concurrently generates a tailored pipeline schedule on-the-fly, effectively adapting to the fluctuating computational demands of multimodal data. This process, which includes data prefetching and schedule searching, runs asynchronously on idle CPU resources, parallel to the main training workers on GPUs. By staying off the critical path, our approach provides the adaptability needed for dynamic data without introducing significant overhead.

**Modality-Aware Partitioning.** The primary source of inefficiency in LMM training stems from the dynamic computational imbalance between different modality modules, as discussed in §2.2. Such dynamic imbalance creates irregular stage latencies and makes it difficult to remove pipeline bubbles. To address this, DIP aims to reduce pipeline bubbles at their source by minimizing stage latency discrepancies. This

is achieved through partitioning the computation of different modality modules into equally-wide *pipeline segments*. Our approach is guided by two key techniques:

① **Remove Intra-Segment Imbalance with Separated Partitioning.** A *pipeline segment* is a set of consecutive stages distributed across all  $P$  pipeline ranks. For example, the four forward stages numbered with “3” in Fig. 5a form one pipeline segment, while their corresponding backward stages form another one. We observe that co-locating stages from different modality modules within the same segment (Fig. 5a) is inherently inefficient. Because vision and language stages have different computational costs and sensitivities to data proportions (e.g., number of images vs. tokens), mixing them creates unavoidable latency disparities between pipeline ranks. Our first principle is to enforce *separated partitioning* (Fig. 5b), where each modality module occupies its own dedicated pipeline segments. This eliminates a primary source of pipeline bubbles. For the ViT 2B + LM 5B model (§2.2), this strategy alone improves performance by 13.1% over the best mixed partitioning scheme.

② **Remove Inter-Segment Imbalance with Modality-Aware Batching.** After separating modalities, we must balance the workload between their respective segments. Our second principle is to partition data within a microbatch into smaller, modality-specific *sub-microbatches* (Fig. 5c). For example, if the entire vision encoder stage is slower than a LM stage, we can process images in smaller sub-microbatches. This allows the encoder to execute multiple shorter stages, and each encoder stage latency can be tailored to better match the latency of a single LM stage. This modality-aware batching reduces latency discrepancies across the entire pipeline, enabling a more globally balanced and efficient schedule.

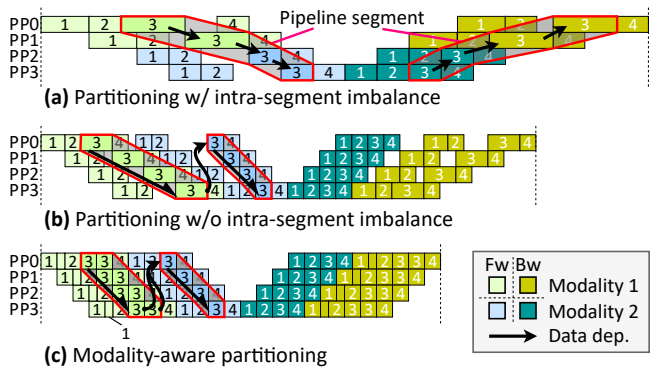


**Figure 5.** Illustrations of partitioning schemes from §3.1. Numbers in boxes denote microbatches. (a) Non-modality-aware partitioning co-locates stages from different modalities in the same pipeline segment, causing intra-segment imbalance. (b) Separated partitioning dedicates distinct pipeline segments to each modality, removing intra-segment imbalance. (c) Modality-aware data batching further splits microbatches into smaller, modality-specific sub-microbatches to balance workloads across segments.

**Decomposed and Scalable Schedule Search.** The scheduling search problem can be formulated as a monolithic integer linear program (ILP) and solved with off-the-shelf solvers [34, 41]. This approach is precise but intractable for real-time use, often taking minutes or hours to solve [16]. To meet the tight time budget of a single training iteration (typically 10–60 seconds, Fig. 8b), we adopt a divide-and-conquer strategy that decomposes the complex search problem into a sequence of simpler, more manageable subproblems. As shown in Fig. 7, our searcher iterates through a three-phase loop, applying tailored heuristics at each step:

① **Pipeline Segment Reordering (§5.1):** First, we determine the optimal processing sequence of pipeline segments. We use Monte Carlo Tree Search (MCTS) to efficiently explore the vast permutation space and identify promising pipeline segment orderings.

② **Pipeline Stage Interleaving (§5.2):** With a fixed segment order, we then arrange the corresponding forward and backward pipeline stages. A fast, dual-queue greedy algorithm interleaves these stages to minimize pipeline bubbles and pack the schedule tightly.

③ **Per-Layer Memory Optimization (§5.3):** Finally, with the schedule structure fixed, we optimize memory usage independently on each pipeline rank. This phase selects memory-saving strategies (e.g., activation checkpointing and offloading) for all model layers to minimize memory usage fluctuations induced by data dynamicity and optimize end-to-end iteration latencies.

This entire loop is highly parallelizable across CPU threads, ensuring that our search process scales with available CPU resources and can serve large distributed training clusters.

### 3.2 System Workflow

The principles above are orchestrated by the DIP training planner, which consists of three main components: modality-aware partitioner (§4), pipeline schedule searcher (§5), and training simulator (§6.1).

The overall workflow proceeds in two phases, as shown in Fig. 6. The modality-aware partitioner comprises an offline model chunk partitioner and an online sub-microbatch partitioner. **Before training**, the model chunk partitioner divides the LMM into model chunks based on our separated partitioning principle and distributes them to the designated GPUs. **During training**, all model chunks remain statically placed on their respective GPU workers, which also fixes the underlying network topology (e.g., NCCL connections). For each iteration, the planner executes a four-stage process:

① **Metadata Prefetching:** The planner fetches metadata for the next batch (e.g., token counts, number of images).

② **Adaptive Microbatch Partitioning:** Using this metadata, the sub-microbatch partitioner divides the microbatches into smaller, modality-specific sub-microbatches to enable inter-segment load balancing.

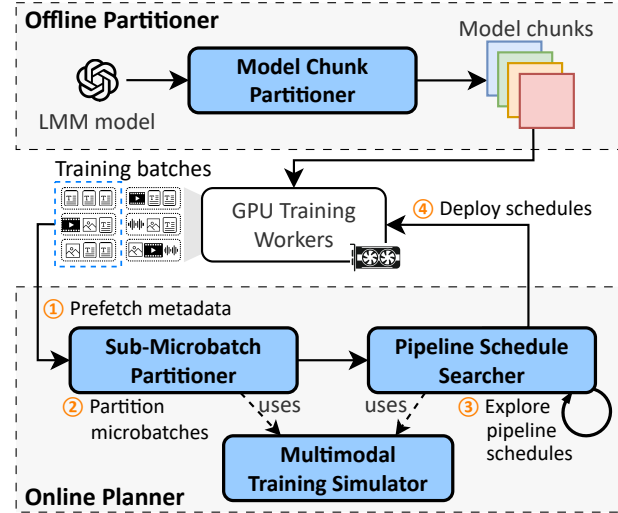


**Figure 6.** The overall workflow of DIP. Before training, the LMM model is partitioned into model chunks by the model chunk partitioner. During each training iteration, DIP asynchronously executes a four-stage online planning process.

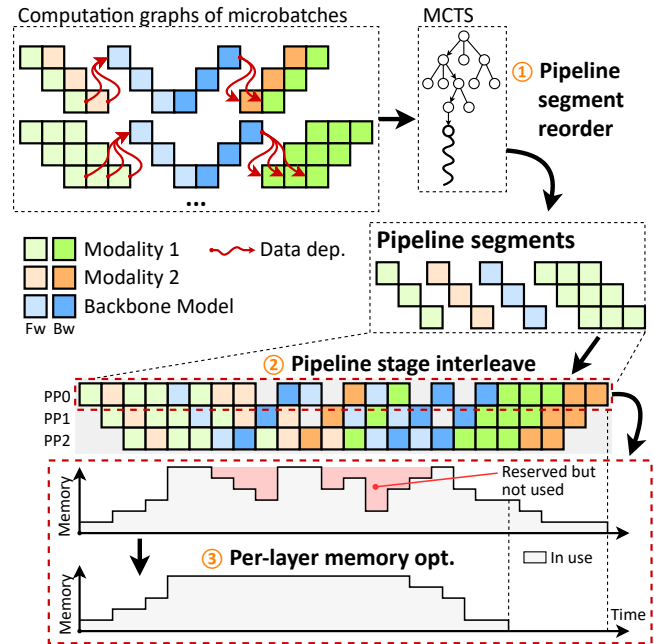


**Figure 7.** The workflow of DIP's pipeline schedule searcher.

③ **Pipeline Schedule Search:** Pipeline schedule searcher is guided by performance estimates from the simulator and runs its three-phase algorithm to find an optimal schedule for the generated sub-microbatches.

④ **Runtime Deployment:** The best schedule is compiled into an execution plan and dispatched to the distributed training runtime for execution.

## 4 Modality-Aware Partitioner

Building on the principles in §3.1, we propose *modality-aware partitioning*. This approach partitions each modality module into multiple model chunks before training, and dynamically splits microbatches into modality-specific sub-microbatches during training. Specifically, for the  $i$ -th modality, DIP determines two parameters: the sub-microbatch size  $B_i$  and the number of pipeline segments  $K_i$ . Consequently, the  $i$ -th modality module is partitioned into  $P \cdot K_i$  model chunks, distributed across  $P$  pipeline ranks.

**Determine Sub-Microbatch Size.** DIP independently selects the minimum viable sub-microbatch size  $B_i$  for each modality module through systematic profiling. Although smaller sub-microbatch sizes enable finer-grained pipeline partitioning and higher scheduling efficiency, excessively small sizes may lead to GPU underutilization (Fig. 9). To balance these trade-offs, DIP measures the computation latency of each modality module across varying sub-microbatch sizes. The optimal  $B_i$  is determined as the smallest sub-microbatch size that maintains at least 95% of the peak GPU computational efficiency observed across all tested configurations.

**Partition Model Chunks.** After determining sub-microbatch sizes, DIP partitions each modality module to achieve global latency balancing. Given  $n$  modality modules with sorted computation latencies  $T_1 \leq T_2 \leq \dots \leq T_n$  (measured at their respective  $B_i$  sizes), DIP assigns pipeline segment counts proportional to these latencies. Specifically, the fastest module ( $T_1$ ) is configured as a single pipeline segment, while the  $i$ -th module is partitioned into  $K_i = \lfloor T_i/T_1 \rfloor$  segments. For a modality module comprising  $L_i$  layers, DIP distributes layers across  $P \cdot K_i$  model chunks, with each chunk containing  $L_i/(P \cdot K_i)$  consecutive layers.

**Construct Sub-Microbatch.** During training execution, DIP dynamically constructs sub-microbatches for each modality module based on the content of incoming microbatches. For a microbatch assigned to the  $i$ -th modality module with  $N_i$  instances, DIP splits it into  $M_i = \lceil N_i/B_i \rceil$  uniformly partitioned sub-microbatches. This process generates  $2M_i \cdot K_i$  pipeline segments in total (accounting for both forward and backward computations) for the modality module.

## 5 Pipeline Schedule Searcher

### 5.1 MCTS-Based Pipeline Segment Reordering

DIP determines the relative ordering between pipeline segments by assigning scheduling priorities to them. These priorities are subsequently utilized in the pipeline stage interleaving phase (§5.2). To efficiently explore the search space of possible priority assignments, DIP employs Monte Carlo tree search (MCTS) [9].

**Search Tree Construction.** Given  $n$  pipeline segments, MCTS constructs a sequence of length  $n$  by iteratively selecting the segment for each position  $i$  (from 1 to  $n$ ). The segment

at the  $i$ -th position receives a priority of  $n-i$ , ensuring earlier selected segments obtain higher priorities.

The algorithm builds a search tree where each node at depth  $d$  corresponds to the  $d$ -th element in the sequence. Consequently, any root-to-node path ending at depth  $d$  represents a partial sequence for the first  $d$  positions. Each node  $v$  maintains the highest performance score  $s_v$  observed among its descendants in the MCTS tree.

**Search Loop.** MCTS iteratively performs the following four phases until convergence:

1. **Node Selection:** Starting from the root, MCTS navigates downward by selecting child nodes that maximize the upper confidence bound (UCB) score  $s_v^\alpha + \beta\sqrt{(\log N_x)/N_v}$ . Here,  $x$  denotes the current node,  $v$  is the target child node,  $N_x$  and  $N_v$  are visit counts, and  $\alpha, \beta$  are hyperparameters. This process repeats until a leaf node  $u$  is reached.
2. **Tree Expansion:** A new node representing the next element after  $u$  is added to the search tree. Then  $u$  is set to the newly created node.
3. **Random Rollouts:** Multiple rollouts (e.g., 10 trials) generate complete sequences by randomly assigning segments to remaining positions after  $u$ . Each sequence then undergoes pipeline stage interleaving (§5.2) and per-layer memory optimization (§5.3) to compute performance scores (i.e., end-to-end iteration time).
4. **Score Backpropagation:** The best rollout score among all trials propagates upward from  $u$  to update the performance scores of ancestor nodes.

This loop continues until either a predefined time budget is exhausted or the entire search space is explored.

**Optimization.** We observe that segments processing the same modality within a single microbatch have identical pipeline structures and similar stage latencies. Consequently, their relative ordering does not impact end-to-end performance. This insight allows DIP to assign identical priorities to such segments and enforce a fixed ordering between them, significantly reducing the search space.

### 5.2 Greedy Pipeline Stage Interleaving

After assigning priorities to segments, DIP employs a dual-queue algorithm to adaptively interleave forward and backward pipeline stages. When both schedulable forward and backward stages are available, DIP mimics Megatron-LM’s memory-efficient “one-forward-one-backward” (1F1B) pattern [24, 39]. When either type is unavailable, a greedy strategy fills pipeline bubbles to construct compact schedules.

**Initialization.** DIP first obtains the stage latencies and memory consumptions for all stages via the training simulator, using the most memory-efficient scheme determined in §5.3. This step ensures sufficient optimization space for subsequent per-layer memory optimizations.

For each pipeline rank, DIP maintains: (1) the end time of the last scheduled stage ( $t_{\text{last}}$ , initially zero); (2) two priority queues ( $Q_{\text{fw}}$ ,  $Q_{\text{bw}}$ ) storing forward and backward stages in descending priority order; and (3) the minimum start time ( $t_{\text{min}}$ ) among stages in  $Q_{\text{fw}}$  and  $Q_{\text{bw}}$ . Each stage maintains a minimum schedulable start time ( $t_{\text{start}}$ ) initialized to zero for stages with no predecessors and  $+\infty$  otherwise.

**Iterative Scheduling.** DIP iteratively selects a pipeline rank and schedules one stage from it:

1. Select the pipeline rank with the smallest  $t_{\text{min}}$ .
2. Compare the minimum start times of stages in  $Q_{\text{fw}}$  ( $t_{\text{fw}}$ ) and  $Q_{\text{bw}}$  ( $t_{\text{bw}}$ ) against  $t_{\text{last}}$ .
3. If both  $t_{\text{fw}} < t_{\text{last}}$  and  $t_{\text{bw}} < t_{\text{last}}$ , schedule alternating forward/backward stages based on the last scheduled stage’s computation type, emulating the 1F1B pattern.
4. Otherwise, select the stage with the smallest  $t_{\text{start}}$  to minimize pipeline bubble between  $t_{\text{min}}$  and stage’s start time.

The selected stage is dequeued and scheduled on the pipeline rank. Subsequently,  $t_{\text{last}}$ ,  $t_{\text{min}}$ , and  $t_{\text{start}}$  values for all successor stages are updated.

**Memory Constraints.** Throughout scheduling, DIP tracks real-time memory consumption across pipeline ranks. When a rank exceeds memory capacity, its forward queue is temporarily disabled to prevent memory overflow.

### 5.3 Per-Layer Memory Optimization

DIP adaptively selects appropriate memory optimization strategies (e.g., activation checkpointing) for all model layers. Since the stage interleaving scheme is predetermined by the dual-queue algorithm (§5.2), this phase independently optimizes end-to-end latency for each pipeline rank.

**Offline Candidate Generation.** Before training, DIP enumerates all possible optimization strategies for each model layer and estimates their execution time and memory consumption using a training simulator. The system then groups each forward stage with its corresponding backward stage into a *stage pair*. For each stage pair, DIP selects up to  $S$  candidate strategies (e.g.,  $S = 10$ ) from the combinatorial space of layer-wise strategies through a three-step process: (1) identifying the fastest candidate, (2) identifying the most memory-efficient candidate, and (3) evenly partitioning the memory range between these extremes into  $S - 2$  buckets, then selecting the most time-efficient candidate within each bucket via a multiple-choice knapsack algorithm [1].

**ILP Formulation.** For each pipeline rank, DIP employs an ILP solver to select optimal candidates. Given  $n$  stage pairs, each with  $S$  candidate strategies, let  $s_i$ ,  $t_i$  denote the start and end timestamps of the  $i$ -th stage pair, and  $\text{lat}_{i,j}$ ,  $\text{mem}_{i,j}$  denote the stage latency and memory consumption of the  $j$ -th candidate for the  $i$ -th stage pair. The formulation uses:

- **Variables:**  $o_{i,j} \in \{0, 1\}$  indicating whether the  $j$ -th candidate is selected for the  $i$ -th stage pair.

- **Objective:** Minimize total latency  $\sum_i \sum_j^S o_{i,j} \cdot \text{lat}_{i,j}$ .
- **Selection Constraints:** Each stage pair selects exactly one strategy, i.e.,  $\sum_j^S o_{i,j} = 1$  ( $\forall 1 \leq i \leq n$ ).
- **Memory Constraints:** At any time  $s_k$ , the memory limit  $M$  is satisfied, i.e.,  $\sum_i^n [s_i \leq s_k \leq t_i] \sum_j^S o_{i,j} \cdot \text{mem}_{i,j} \leq M$  ( $\forall 1 \leq k \leq n$ ), where  $[\cdot]$  is the Iverson bracket [21].

**Optimizations.** Although the problem scale has been significantly reduced compared to the monolithic, end-to-end ILP formulation, solving an ILP instance may still require several seconds. We introduce two techniques to achieve efficient solving ( $<10$  ms per instance on a single CPU core): (1) warm-starting the ILP solver with a greedy initial solution, and (2) permitting a small optimality gap (e.g.,  $\leq 5\%$ ) for early termination, as closing the final 5% gap incurs diminishing returns but prohibitive computational costs.

### 5.4 Time Complexity Analysis

In this section, we outline the algorithmic structure of DIP’s training planner and analyze its time complexity. The planner operates as an iterative search loop that continues until a predefined time budget is exhausted. Each iteration consists of three stages: pipeline segment reordering (§5.1), pipeline stage interleaving (§5.2), and per-layer memory optimization (§5.3). For the complexity analysis of a single search iteration, let  $p$  denote the number of pipeline ranks,  $n$  the number of sub-microbatches, and  $S$  the number of candidate memory-saving strategies. Additionally, let  $\text{ApproxILP}(m, k)$  represent the time complexity of the approximate ILP solver for an instance with  $O(m)$  variables and  $O(k)$  constraints.

First, pipeline segment reordering generates an ordering for all sub-microbatches in  $O(n)$  time. Second, the greedy scheduling algorithm for pipeline stage interleaving runs in time proportional to the total number of pipeline stages, i.e.,  $O(p \cdot n)$ . Finally, per-layer memory optimization solves a set of small, approximate ILP instances to select the optimal configuration for each pipeline rank. Each ILP instance requires creating  $n \cdot S$  indicator variables ( $o_{i,j}$ ), along with  $n$  selection constraints and  $n$  memory constraints. Consequently, the time complexity for per-layer memory optimization is  $O(p \cdot \text{ApproxILP}(n \cdot S, n))$ . Combining all these steps, the overall time complexity for a single search iteration is  $O(p \cdot (n + \text{ApproxILP}(n \cdot S, n)))$ .

In contrast, a full ILP baseline approach is inherently inefficient due to the massive scale of variables and constraints involved. First, it requires solving the entire pipeline globally, rather than decomposing the problem per pipeline rank. Second, it necessitates  $O(n^2)$  ordering constraints to prevent overlapping stage executions within each pipeline rank, whereas DIP avoids this overhead through efficient explicit scheduling. Furthermore, in the memory optimization phase, assuming  $L$  layers per pipeline stage and  $c$  candidate strategies per layer, the search space expands to  $c^L$  candidates per stage. Consequently, the complexity of the baseline ILP

**Table 2.** Model specifications used in the evaluation.

Name	# of Layers	Embed Dim	FFN Hidden Dim	# of Attn. Heads	# of Attn. Groups
ViT 5B [12]	63	1792	15360	16	16
ViT 22B [12]	48	6144	24576	48	48
Llama3 8B [17]	32	4096	14336	32	8
Qwen2 32B [51]	64	5120	27648	40	8
Qwen2 72B [51]	80	8192	29568	64	8
DiT 5B [35]	28	3584	10240	28	28
DiT 30B [35]	48	6144	24576	48	48

**Table 3.** Model combinations used in the evaluation.

Name	Model Setup	TP	PP	#GPU
VLM-S	ViT 5B + Llama3 8B	4	4	16
VLM-M	ViT 5B + Qwen2 32B	8	4	32
VLM-L	ViT 22B + Qwen2 72B	8	8	64
T2V-S	Llama3 8B + DiT 5B	4	4	16
T2V-L	Qwen2 32B + DiT 30B	8	8	64

approach escalates to  $O(\text{ApproxILP}(p \cdot n \cdot c^L, p \cdot n^2))$ . We empirically compare the performance of this baseline against DIP’s training planner in §7.4 and Fig. 12.

## 6 Implementation

DIP is implemented as an extension to Megatron-LM [39], featuring a central planner that coordinates with Megatron-LM’s runtime. The planner iteratively prefetches training metadata, performs pipeline schedule searches, and deploys the optimized schedules to GPU clusters.

### 6.1 Training Simulator

DIP employs operator-level analytical modeling for performance prediction. The simulator constructs directed acyclic graphs (DAGs) with two node types: (1) operator nodes representing low-level GPU operations (e.g., matrix multiplication, collective communication), and (2) tensor nodes corresponding to data buffers (e.g., model parameters). Each node is assigned to a specific device (GPU/CPU/NVLink) and connected with dependency edges.

For latency estimation, each operator node is characterized by: the number of floating-point operations  $N_{\text{fop}}$ , memory accesses  $N_{\text{mem}}$  in bytes, and network transfers  $N_{\text{net}}$  in bytes. Given device capabilities (computational capacity  $F$  in FLOPS, memory bandwidth  $B_{\text{mem}}$  in bytes/s, and network throughput  $B_{\text{net}}$  in bytes/s), the latency is computed as  $\max\{\alpha_{\text{fop}}N_{\text{fop}}/F, \alpha_{\text{mem}}N_{\text{mem}}/B_{\text{mem}}, \alpha_{\text{net}}N_{\text{net}}/B_{\text{net}}\}$ , where  $\alpha_{\text{fop}}$ ,  $\alpha_{\text{mem}}$ , and  $\alpha_{\text{net}}$  are efficiency scaling factors. Users may override this cost model with custom estimation rules.

The simulator populates operator timestamps in topological order, then determines tensor lifetimes by examining related operator nodes. These lifetimes enable construction of memory consumption timelines for peak memory usage estimation across devices.

### 6.2 Parallel Schedule Search

DIP executes the training simulator and search algorithms on CPU cores. It begins by simulating individual microbatch computation graphs using prefetched metadata to obtain pipeline stage latencies. During schedule search, multiple workers explore the schedule space in parallel while sharing global MCTS search statistics. After each search round, these workers atomically update the global MCTS statistics via mutex-protected operations. Contention remains minimal because workers perform multiple rollouts between synchronizations, thereby amortizing the overhead. To avoid interference with normal training processes, DIP constrains the search worker count to at most 50% of available CPU cores (e.g., 64 cores on a machine with 8 H800 GPUs).

### 6.3 Execution Plan Deployment

Deploying simulated pipeline schedules to GPU clusters requires compiling them into physical execution plans that specify computation and communication patterns.

**Schedule Compilation.** DIP defines action sequences constituting pipeline execution plans, following DynaPipe [24]:

- Pipeline stages translate to `fw_stage/bw_stage` actions with optimization strategies from §5.3.
- Point-to-point (P2P) communications use asynchronous kernels (`isend`, `irecv`) overlapped with computations.
- Synchronization actions (`wait_isend`, `wait_irecv`) are inserted based on simulated timelines.

**Runtime Modifications.** We extend Megatron-LM’s schedules module to support dynamic plans. Each pipeline worker receives an action list via RPC from the central planner and executes it sequentially. Consecutive P2P kernels are grouped into a batched operation to enhance efficiency.

## 7 Evaluation

### 7.1 Methodology

**Models.** We conduct comprehensive evaluations of DIP across two major LMM architectures: vision-language models (VLMs) and text-to-video (T2V) models (Table 2). The VLM architectures integrate ViT-based image encoders (5B and 22B parameters) [12, 14] with language model backbones (Llama3 8B [17], Qwen2 32B/72B [50]), while T2V architectures combine language model encoders with DiT-based diffusion video decoders (5B and 30B parameters) [35]. We choose five distinct model combinations ranging from 12B to 94B parameters, as detailed in Table 3.

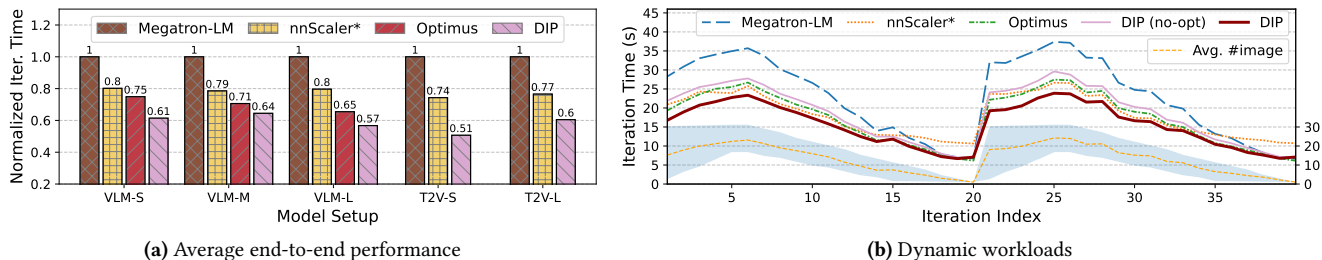


**Figure 8.** End-to-end performance. (a) Average performance of 100 iteration on real datasets across five model setups. (b) End-to-end latency timeline of 40 consecutive iterations. The orange dashed line depicts the average number of images.

**Datasets.** We employ a combination of diverse open-source datasets [4, 7, 25, 30, 38, 46], comprising pure image-text pairs, interleaved image-text documents, and video-caption pairs. For VLM models, we adopt the ViT architecture used in Qwen2 VL [45]. We scale all images to 728px resolution, with each image being encoded by the ViT vision encoder into 169 patch tokens ( $\text{patch\_size}=14$ ,  $\text{spatial\_merge\_size}=4$ ). Multiple image-text data samples are packed into sequences of 8192 tokens, resulting in a maximum image capacity of  $\lceil 8192/169 \rceil = 48$  per sequence. For T2V models, we adopt MovieGen’s [35] configuration by transcoding videos to 16 FPS with a maximum duration of 16 seconds. When processing short videos, we group up to 8 video clips per microbatch while maintaining the total microbatch duration below 16 seconds.

**Baselines.** We benchmark DIP against four state-of-the-art baseline systems:

- **Fully Sharded Data Parallel (FSDP)** [55] is a memory-efficient training strategy standard in PyTorch. It shards model parameters, gradients, and optimizer states across data parallel workers, collecting them via communication only during the computation of the current layer. We employ FSDP2 in PyTorch 2.8.0 with ZeRO-3 configuration ( $\text{reshard\_after\_forward}=\text{true}$ ) for Transformer blocks to minimize peak memory usage.
- **Megatron-LM** [39] is a widely-used unimodal LLM training framework. We use interleaved pipeline parallelism (VPP) and partition LMM layers into model chunks with approximately balanced parameter distribution.
- **nnScaler** [28] automates parallelization for deep neural network training. Since generating a single parallelization plan takes several minutes and requires a restart of the training process for plan updates, we pre-generate a static parallelization plan before training with a representative training workload. For fair cross-framework comparison, we implement nnScaler’s model chunk partitioning schemes and memory optimizations in Megatron-LM, with performance metrics labeled as “nnScaler\*”.
- **Optimus** [15] proposes coarse-grained and fine-grained bubble scheduling to optimize multimodal LLM (MLLM)

training with multiple encoders. The coarse-grained strategy sequences all modality encoder computations before backbone model execution at the pipeline level, while the fine-grained method fills TP communication bubbles with encoder computations and is orthogonal to our pipeline design. For focused pipeline scheduling comparisons, we implement Optimus’ coarse-grained bubble scheduling in DIP. Due to the lack of support for diffusion decoders, we exclude Optimus from T2V model evaluations.

Spindle [47] is excluded from the evaluation primarily because it is tailored for static, multi-task scenarios where tasks must be pre-defined prior to training. This static design fundamentally contrasts with the dynamic and flexible input-handling capabilities required by modern LLMs.

**Testbed.** We conducted large-scale experiments on a cluster of 64 NVIDIA 80GB H800 GPUs distributed across 8 nodes. Each node is equipped with 128 CPU cores, 256GB of host memory, and 8 H800 GPUs interconnected via 200 GB/s NVLink. Inter-node communication relies on an 8×200Gbps RoCEv2 network with a rail-optimized topology. Additionally, a smaller cluster consisting of two nodes, each populated with 8 NVIDIA 96GB H20 GPUs, was utilized for comparative baselines against FSDP and Megatron-LM.

**Metrics.** We adopt training iteration time and model FLOPs utilization (MFU) as performance metrics, with all reported values averaged across 10 independent runs.

## 7.2 End-to-End Performance

**Comparison with LLM Training Systems.** We begin by benchmarking DIP against FSDP and Megatron-LM, both of which are widely adopted frameworks for unimodal LLM training. These experiments were conducted on the 16-GPU H20 cluster, leveraging the large 96GB VRAM per GPU to minimize activation recomputation overhead. As shown in Table 4, FSDP is only 3% slower than Megatron-LM, whereas DIP achieves a 27% speedup over Megatron-LM. Given the marginal performance gap between FSDP and Megatron-LM, we implement all remaining baselines based on Megatron-LM to ensure a fair cross-framework comparison.

**Table 4.** VLM-S end-to-end performance of FSDP, Megatron-LM, and DIP on 16 H20 GPUs.

	FSDP [55]	Megatron-LM [39]	DIP
Iteration time (s)	40.270	39.053	28.606
Relative time	1.03	1.00	0.73

**Comparison with Multimodal Training Systems.** We conduct experiments comparing the average end-to-end performance of DIP against baseline systems using real datasets and five model configurations summarized in Table 3. As demonstrated in Fig. 8a, DIP achieves training throughput improvements of 15.6%–76.2% over three baseline systems in VLM model setups, and 36.6%–97.3% over two baselines in T2V model configurations, demonstrating consistent performance gains across diverse model architectures and parameter scales.

**Dynamic Workloads.** To analyze DIP’s performance characteristics under dynamic workloads against other baselines, we investigate the VLM-S model with manual control of image count bounds during training iterations. We monitor 40 iterations showing two "rise-and-fall" patterns in image counts. Each pattern consists of: (1) gradually increasing the lower bound from 0 to 16 while maintaining an upper bound of 32 (iterations 1–5), achieving a peak average of 22 images, followed by (2) progressively reducing both bounds to zero (iterations 6–20).

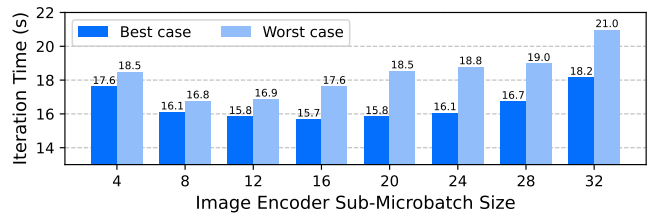
Fig. 8b reveals DIP’s consistent superior performance across all systems. During high-image-count phases (iterations 1–10), Megatron-LM suffers significant computational imbalance across modality modules and data microbatches, exhibiting a 52.9% slowdown compared to DIP at iteration 6. Although both nnScaler and Optimus partially mitigate dynamic imbalance effects, they are still 10.4% slower than DIP. As both image counts and bound gaps decrease (iterations 11–20), training workloads converge toward pure language tasks, narrowing the performance gap between DIP and baseline systems. Notably, nnScaler’s restriction to 1F1B scheduling mandates all modality modules to be partitioned inside one pipeline segment, which creates significant pipeline imbalance when image encoder workloads diminish, resulting in 50.5% performance degradation during iterations 15–20.

### 7.3 Performance Ablation

**Performance Breakdown.** Using the VLM-S model setup, we incrementally integrate four key components (modality-aware partitioner, pipeline stage interleaving, segment reordering, and per-layer memory optimization) onto Megatron-LM. As demonstrated in Table 5, the modality-aware partitioner alone delivers a 17.3% performance improvement over the baseline Megatron-LM, highlighting its critical role in LMM training. Among optimizations of pipeline schedule

**Table 5.** Quantitative impact of DIP’s optimizations.

Techniques	Iter. Time (s)	$\Delta\%$
Vanilla Megatron-LM	26.13	0.0%
+ Modality-aware partitioner (§4)	22.27	17.3%
+ Pipeline stage interleaving (§5.2)	18.81	38.9%
+ Pipeline segment reordering (§5.1)	17.61	48.3%
+ Pre-layer memory optimization (§5.3)	16.05	62.8%

**Figure 9.** Impact of sub-microbatch sizes.

searcher, pipeline stage interleaving provides a substantial 21.6% performance boost compared to Megatron-LM’s default pipelining. Subsequent segment reordering and per-layer memory optimization enhance performance by an additional 23.9% via intelligent reordering of pipeline segments and adaptive memory optimization strategy selection. In Fig. 8b, we visually contrast improvements from modality-aware partitioner and pipeline schedule searcher over dynamic workloads, separated by the line labeled “DIP (no-opt)” that excludes pipeline schedule searcher’s optimizations.

**Impact of Sub-Microbatch Sizes.** We investigate the influence of modality-specific sub-microbatch sizes on pipeline scheduling and GPU execution efficiency using the VLM-S model, by testing image sub-microbatch sizes ranging from 4 to 32 and deriving the best and the worst<sup>1</sup> pipeline schedules.

Our analysis of Fig. 9 reveals two key findings. First, smaller sub-microbatch sizes (4–12) significantly reduce the performance gap between best and worst schedules from 15.4% to 5.1%. This narrowed variance indicates reduced sensitivity to schedule configurations, thereby lowering the difficulty in achieving optimal pipeline schedules. Second, extremely small sub-microbatch sizes (<8) demonstrate diminishing returns due to underutilized GPU computational capacity, resulting in a 12.1% increase in iteration time compared to medium-sized batches. Through empirical validation, we identify a sub-microbatch size of 12 as the optimal balance point between pipeline schedule flexibility and hardware utilization efficiency.

**Impact of Per-Layer Memory Optimization.** We analyze the memory usage timeline of the first pipeline rank during VLM-M model training. As shown in Fig. 10, baseline

<sup>1</sup>We obtain the worst pipeline schedule by inverting the optimization goal of pipeline schedule searcher to maximizing iteration time.

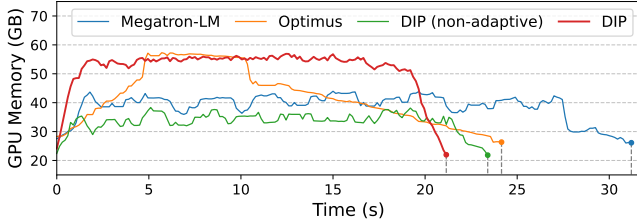


**Figure 10.** Memory usage timelines of the first pipeline rank in VLM-M training. The “DIP (non-adaptive)” disables per-layer memory optimization and does not utilize all available GPU memory.

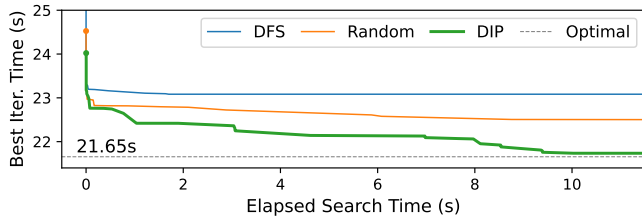


**Figure 11.** Search progress of different exploration strategies.

systems fail to fully utilize available GPU memory. Megatron-LM exhibits significant memory fluctuations during the steady 1F1B pipeline phase, while Optimus manifests a gradual memory increase due to executing all modality encoder computations and storing substantial activation memory prior to the backbone model. This results in 25.3% higher peak memory consumption compared to Megatron-LM. In contrast, DIP maintains consistently low memory usage throughout training iterations by partitioning microbatches into smaller sub-microbatches, enabling finer-grained interleaving of forward and backward pipeline stages. Per-layer memory optimization further intelligently selects memory optimization configurations to achieve full utilization of available GPU memory, achieving 52.9% fewer memory fluctuations than Megatron-LM and delivering 12.2% performance gains over Optimus under equivalent peak memory conditions.

### 7.4 Planner Evaluation

**Search Efficiency.** To demonstrate the efficiency of DIP’s pipeline schedule search, we track the progression of current best pipeline schedule performance versus elapsed search time, comparing it with two variants using depth-first search (DFS) and random exploration instead of MCTS algorithm. Using the largest VLM-L model as the target workload, we run all search algorithm variants on 64 CPU cores. Fig. 11 shows DIP achieves near-optimal pipeline schedule performance within 10 seconds, which can be overlapped with VLM-L’s typical 20-second training iteration duration. In contrast, DFS and random exploration strategies fail to quickly identify optimal pipeline schedules due to their lack of guided search optimization with performance scores like MCTS.

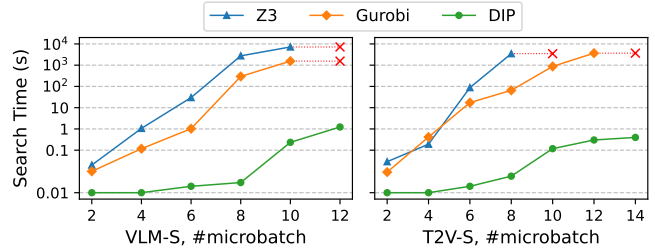


**Figure 12.** Search time comparison of Z3, Gurobi, and DIP across varying microbatch counts for VLM-S and T2V-S. The Y-axis is plotted on a log scale. Red crosses (×) indicate timeouts (>3 hours).

**Search Scalability.** We evaluate search scalability using two model configurations: VLM-S and T2V-S. Specifically, we measure the search latency of DIP as the number of microbatches increases, which correspondingly increases the number of pipeline stages and the complexity of the pipeline schedule. We benchmark DIP against two state-of-the-art SMT/ILP solvers: Z3 [13] and Gurobi [34] (version 13.0). For the experimental setup, both DIP and Gurobi utilize up to 64 CPU threads, whereas Z3 operates on a single thread as it inherently lacks support for multi-threaded solving. As shown in Fig. 12, DIP consistently maintains a search time under 10 seconds. In contrast, the search times for both Z3 and Gurobi exhibit exponential growth with respect to the number of microbatches. Consequently, both solvers cannot complete in 30 minutes when the number of microbatches surpasses 10, rendering them impractical for dynamic pipeline schedule generation in LMM training.

**Simulation Accuracy.** We assess the accuracy of DIP’s training simulator through a grid-search experiment for VLM-M across 64 GPUs, and compare simulated results against actual GPU executions. We systematically evaluate all valid combinations of DP, PP, and TP sizes where all values are powers of two and  $TP \leq 8$ . As illustrated in Fig. 13, the optimal parallelism configuration is DP8, TP2, and PP4, achieving a MFU of 29.7%. Although DIP’s default simulation settings initially exhibit relative errors up to 10% compared to ground-truth measurements, the simulator still successfully predicts the optimal parallel configuration. Through calibration via offline microbenchmarks that align efficiency scaling factors for matrix multiplications and collective communication operations, the training simulator achieves an average simulation accuracy of 97.6%.

### 7.5 Large-Scale Simulation

To validate DIP’s effectiveness in large-scale H100 GPU cluster environments, we conducted two experiments using the training simulator with substantial large multimodal models (VLM-XL and T2V-XL) to evaluate its theoretical improvements over baseline approaches. Detailed configurations for both models and GPU clusters are presented in Table 6.

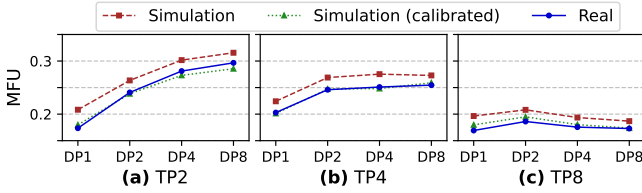


**Figure 13.** Comparison between pre- and post-calibration simulation results versus actual GPU executions.

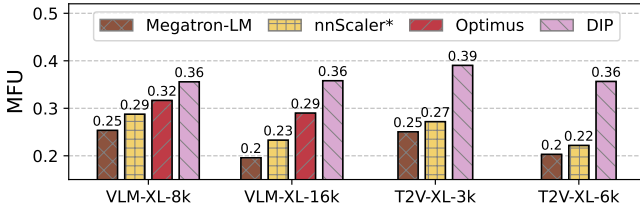


**Figure 14.** Large scale simulations on H100 clusters.

**Results.** Experimental results in Fig. 14 demonstrate that DIP achieves MFU scores of 0.36 for VLM-XL and 0.39 for T2V-XL. The system consistently outperforms baseline methods by up to 82.8%, particularly with larger pipeline parallelism sizes, as larger PP dimensions introduce more complex pipeline structures that require meticulous orchestration between stages by the pipeline schedule searcher.

## 8 Related Work

**Automated Training Parallelization.** Several systems have been proposed to automate parallelization strategies for training deep learning models [28, 43, 56]. These systems perform full-scale model planning across DP, PP, and TP dimensions. Although they employ exhaustive search algorithms to generate near-optimal training configurations, the planning process often incurs substantial time overhead—requiring several minutes to complete [28]. This makes such approaches impractical for LMM training, which demands dynamic and adaptive pipeline scheduling.

**Training Systems for Multimodal Models.** Numerous system optimizations [15, 19, 22, 42, 47, 53, 57] have been developed to address architectural and training data heterogeneity in multimodal model training. For instance, DistMM [19] tackles model and data heterogeneity in traditional CLIP-based models, where all encoders are parallel. However, this design does not generalize to LMMs, which exhibit sequential dependencies between encoders, backbones and decoders. Similarly, both Spindle [47] and Optimus [15] target multimodal LLMs under predefined training tasks, overlooking the inherent dynamicity in LMM training pipelines. Specifically, Spindle is designed for a static, multi-task setting where all tasks are pre-defined before training starts. This contrasts with the dynamic and flexible input-handling capabilities required by modern LMMs, which is the focus of DIP.

**Table 6.** Model combinations used in the large-scale simulation.

Name	Model Setup	DP	TP	PP	#GPU
VLM-XL-8k	ViT 22B + GPT 175B	128	8	8	8192
VLM-XL-16k	ViT 22B + GPT 175B	128	8	16	16384
T2V-XL-3k	Qwen2 72B + DiT 30B	96	8	4	3072
T2V-XL-6k	Qwen2 72B + DiT 30B	96	8	8	6144

**Pipeline Parallelism Scheduling.** Beyond Megatron-LM’s 1F1B schedule, several alternative pipeline schedules have been proposed [23, 26, 29, 36]. Chimera [26] introduces bidirectional pipelines to reduce pipeline bubbles, while zero bubble pipeline [36] further minimizes bubbles by decoupling backward computations into input gradient and weight gradient phases. However, these methods assume fixed pipeline stage latencies and still suffer from the dynamic imbalance problem. GraphPipe [23] targets models with heterogeneous modules by organizing computations into a directed acyclic graph (DAG) rather than sequential stages, enabling more flexible scheduling. DIP’s pipeline schedule searcher can be extended to incorporate such custom schedules like GraphPipe.

**Pipeline with Variable Sequence Lengths.** Several systems address text sequence length variations in unimodal LLM training [5, 24, 48, 52, 54]. For example, DynaPipe [24] optimizes micro-batch construction using dynamic programming for multi-task training. WLB-LLM [48] proposes a fine-grained per-document sharding strategy to balance workloads in context parallelism groups. FlexPipe [54] dynamically adjusts pipeline size via a live flexibility mechanism to reassign GPU workers processing short sequences to assist with longer ones. While these approaches are effective for text-based models, they do not handle multi-modal data. In contrast, our approach supports multiple modalities within a single pipeline.

## 9 Conclusion

Efficient large multimodal model training is challenging due to pipeline stage imbalance and training data dynamicity. In this paper, we propose DIP to address dynamic imbalance of LMM training with adaptive modality-aware partitioning and efficient pipeline schedule search. Our experimental results demonstrate that DIP outperforms existing state-of-the-art training systems by up to 97.3% in training throughput.

## Acknowledgments

We sincerely thank our shepherd Jongsoo Park, and the anonymous reviewers for their insightful suggestions. This work was partially supported by NSFC (No. 62372287 and U24A20235). Zeyu Mi (yzmizeyu@sjtu.edu.cn) is the corresponding author.

## References

- [1] R. D. Armstrong, D. S. Kung, P. Sinha, and A. A. Zoltners. 1983. A Computational Study of a Multiple-Choice Knapsack Algorithm. *ACM Trans. Math. Softw.* 9, 2 (June 1983), 184–198. doi:10.1145/357456.357458
- [2] Shuai Bai, Keqin Chen, Xuejing Liu, Jialin Wang, Wenbin Ge, et al. 2025. Qwen2.5-VL Technical Report. arXiv. arXiv:2502.13923 [cs.CV] <https://arxiv.org/abs/2502.13923>
- [3] Minwoo Byeon, Beomhee Park, Haecheon Kim, Sungjun Lee, Woonhyuk Baek, et al. 2022. COYO-700M: Image-Text Pair Dataset. <https://github.com/kakaobrain/coyo-dataset>.
- [4] Lin Chen, Xilin Wei, Jinsong Li, Xiaoyi Dong, Pan Zhang, et al. 2024. ShareGPT4Video: Improving Video Understanding and Generation with Better Captions. arXiv. arXiv:2406.04325 [cs.CV] <https://arxiv.org/abs/2406.04325>
- [5] Qiaoling Chen, Shenggui Li, Wei Gao, Peng Sun, Yonggang Wen, et al. 2025. SPPO: Efficient Long-Sequence LLM Training via Adaptive Sequence Pipeline Parallel Offloading. arXiv:2503.10377 [cs.DC] <https://arxiv.org/abs/2503.10377>
- [6] Ting Chen, Simon Kornblith, Mohammad Norouzi, and Geoffrey Hinton. 2020. A Simple Framework for Contrastive Learning of Visual Representations. In *Proceedings of the 37th International Conference on Machine Learning (ICML '20)*. JMLR.org, Virtual conference, Article 149, 11 pages.
- [7] Xiaowei Chi, Yatian Wang, Aosong Cheng, Pengjun Fang, Zeyue Tian, et al. 2024. MMTrail: A Multimodal Trailer Video Dataset with Language and Music Descriptions. arXiv. arXiv:2407.20962 [cs.CV] <https://arxiv.org/abs/2407.20962>
- [8] Yew Ken Chia, Liying Cheng, Hou Pong Chan, Chaoqun Liu, Maojia Song, et al. 2024. M-Longdoc: A Benchmark For Multimodal Super-Long Document Understanding And A Retrieval-Aware Tuning Framework. arXiv. arXiv:2411.06176 [cs.CL] <https://arxiv.org/abs/2411.06176>
- [9] Rémi Coulom. 2007. Efficient Selectivity and Backup Operators in Monte-Carlo Tree Search. In *Computers and Games*, H. Jaap van den Herik, Paolo Ciancarini, and H. H. L. M. (Jeroen) Donkers (Eds.). Springer Berlin Heidelberg, Berlin, Heidelberg, 72–83.
- [10] DeepMind. 2025. Gemma 3. <https://blog.google/technology/developer/gemma-3/>.
- [11] DeepSeek-AI, Aixin Liu, Bei Feng, Bing Xue, Bingxuan Wang, et al. 2025. DeepSeek-V3 Technical Report. arXiv:2412.19437 [cs.CL] <https://arxiv.org/abs/2412.19437>
- [12] Mostafa Dehghani, Josip Djolonga, Basil Mustafa, Piotr Padlewski, Jonathan Heek, et al. 2023. Scaling Vision Transformers to 22 Billion Parameters. arXiv. arXiv:2302.05442 [cs.CV] <https://arxiv.org/abs/2302.05442>
- [13] Z3 developers. 2025. The Z3 Theorem Prover. <https://github.com/Z3Prover/z3>.
- [14] Alexey Dosovitskiy, Lucas Beyer, Alexander Kolesnikov, Dirk Weissenborn, Xiaohua Zhai, et al. 2021. An Image is Worth 16x16 Words: Transformers for Image Recognition at Scale. In *International Conference on Learning Representations*. <https://openreview.net/forum?id=YicbFdNTTy>
- [15] Weiqi Feng, Yangrui Chen, Shaoyu Wang, Yanghua Peng, Haibin Lin, et al. 2025. Optimus: Accelerating Large-Scale Multi-Modal LLM Training by Bubble Exploitation. In *2025 USENIX Annual Technical Conference (USENIX ATC 25)*. USENIX Association, Boston, MA, USA, 161–178.
- [16] Swapnil Gandhi, Mark Zhao, Athinagoras Skiadopoulos, and Christos Kozyrakis. 2024. ReCycle: Resilient Training of Large DNNs using Pipeline Adaptation. In *Proceedings of the ACM SIGOPS 30th Symposium on Operating Systems Principles (Austin, TX, USA) (SOSP '24)*. Association for Computing Machinery, New York, NY, USA, 211–228. doi:10.1145/3694715.3695960
- [17] Aaron Grattafiori, Abhimanyu Dubey, Abhinav Jauhri, Abhinav Pandey, Abhishek Kadian, et al. 2024. The Llama 3 Herd of Models. arXiv:2407.21783 [cs.AI] <https://arxiv.org/abs/2407.21783>
- [18] Ailin Huang, Boyong Wu, Bruce Wang, Chao Yan, Chen Hu, et al. 2025. Step-Audio: Unified Understanding and Generation in Intelligent Speech Interaction. arXiv. arXiv:2502.11946 [cs.CL] <https://arxiv.org/abs/2502.11946>
- [19] Jun Huang, Zhen Zhang, Shuai Zheng, Feng Qin, and Yida Wang. 2024. DISTMM: Accelerating Distributed Multimodal Model Training. In *21st USENIX Symposium on Networked Systems Design and Implementation (NSDI 24)*. USENIX Association, Santa Clara, CA, 1157–1171. <https://www.usenix.org/conference/nsdi24/presentation/huang>
- [20] Minbin Huang, Yanxin Long, Xincheng Deng, Ruihang Chu, Jiangfeng Xiong, et al. 2024. DialogGen: Multi-modal Interactive Dialogue System for Multi-turn Text-to-Image Generation. arXiv. arXiv:2403.08857 [cs.CV] <https://arxiv.org/abs/2403.08857>
- [21] Kenneth E. Iverson. 1962. A Programming Language. In *Proceedings of the May 1-3, 1962, Spring Joint Computer Conference* (San Francisco, California) (AIEE-IRE '62 (Spring)). Association for Computing Machinery, New York, NY, USA, 345–351. doi:10.1145/1460833.1460872
- [22] Insu Jang, Runyu Lu, Nikhil Bansal, Ang Chen, and Mosharaf Chowdhury. 2025. Cornstarch: Distributed Multimodal Training Must Be Multimodality-Aware. arXiv. arXiv:2503.11367 [cs.DC] <https://arxiv.org/abs/2503.11367>
- [23] Byungsoo Jeon, Mengdi Wu, Shiyi Cao, Sunghyun Kim, Sunghyun Park, et al. 2025. GraphPipe: Improving Performance and Scalability of DNN Training with Graph Pipeline Parallelism. In *Proceedings of the 30th ACM International Conference on Architectural Support for Programming Languages and Operating Systems, Volume 1 (Rotterdam, Netherlands) (ASPLoS '25)*. Association for Computing Machinery, New York, NY, USA, 557–571. doi:10.1145/3669940.3707220
- [24] Chenyu Jiang, Zhen Jia, Shuai Zheng, Yida Wang, and Chuan Wu. 2024. DynaPipe: Optimizing Multi-Task Training through Dynamic Pipelines. In *Proceedings of the Nineteenth European Conference on Computer Systems (Athens, Greece) (EuroSys '24)*. Association for Computing Machinery, New York, NY, USA, 542–559. doi:10.1145/3627703.3629585
- [25] Hugo Laurençon, Lucile Saulnier, Léo Tronchon, Stas Bekman, Amanpreet Singh, et al. 2023. OBELICS: An Open Web-Scale Filtered Dataset of Interleaved Image-Text Documents. arXiv. arXiv:2306.16527 [cs.IR] <https://arxiv.org/abs/2306.16527>
- [26] Shigang Li and Torsten Hoefler. 2021. Chimera: Efficiently Training Large-Scale Neural Networks with Bidirectional Pipelines. In *Proceedings of the International Conference for High Performance Computing, Networking, Storage and Analysis (St. Louis, Missouri) (SC '21)*. Association for Computing Machinery, New York, NY, USA, Article 27, 14 pages. doi:10.1145/3458817.3476145
- [27] Zhimin Li, Jianwei Zhang, Qin Lin, Jiangfeng Xiong, Yanxin Long, et al. 2024. Hunyuan-DiT: A Powerful Multi-Resolution Diffusion Transformer with Fine-Grained Chinese Understanding. arXiv. arXiv:2405.08748 [cs.CV] <https://arxiv.org/abs/2405.08748>
- [28] Zhiqi Lin, Youshan Miao, Quanlu Zhang, Fan Yang, Yi Zhu, et al. 2024. nnScaler: Constraint-Guided Parallelization Plan Generation for Deep Learning Training. In *18th USENIX Symposium on Operating Systems Design and Implementation (OSDI 24)*.
- [29] Ziming Liu, Shenggan Cheng, Haotian Zhou, and Yang You. 2023. Hanayo: Harnessing Wave-Like Pipeline Parallelism for Enhanced Large Model Training Efficiency. In *Proceedings of the International Conference for High Performance Computing, Networking, Storage and Analysis (Denver, CO, USA) (SC '23)*. Association for Computing Machinery, New York, NY, USA, Article 56, 13 pages. doi:10.1145/3581784.3607073
- [30] Pan Lu, Swaroop Mishra, Tony Xia, Liang Qiu, Kai-Wei Chang, et al. 2022. Learn to Explain: Multimodal Reasoning via Thought Chains for Science Question Answering. In *The 36th Conference on Neural Information Processing Systems (NeurIPS)*.

- [31] Guoqing Ma, Haoyang Huang, Kun Yan, Liangyu Chen, Nan Duan, et al. 2025. Step-Video-T2V Technical Report: The Practice, Challenges, and Future of Video Foundation Model. arXiv. arXiv:2502.10248 [cs.CV] <https://arxiv.org/abs/2502.10248>
- [32] OpenAI. 2024. GPT-4o System Card. <https://openai.com/index/gpt-4o-system-card/>.
- [33] OpenAI. 2025. Introducing 4o Image Generation. <https://openai.com/index/introducing-4o-image-generation/>.
- [34] Gurobi Optimization. 2025. Gurobi. <https://www.gurobi.com/>.
- [35] Adam Polyak, Amit Zohar, Andrew Brown, Andros Tjandra, Animesh Sinha, et al. 2024. Movie Gen: A Cast of Media Foundation Models. arXiv. arXiv:2410.13720 [cs.CV] <https://arxiv.org/abs/2410.13720>
- [36] Penghui Qi, Xinyi Wan, Guangxing Huang, and Min Lin. 2024. Zero Bubble Pipeline Parallelism. In *The Twelfth International Conference on Learning Representations*. <https://openreview.net/forum?id=tuzTNOeIO5>
- [37] Alec Radford, Jong Wook Kim, Chris Hallacy, Aditya Ramesh, Gabriel Goh, et al. 2021. Learning Transferable Visual Models From Natural Language Supervision. arXiv. arXiv:2103.00020 [cs.CV] <https://arxiv.org/abs/2103.00020>
- [38] Christoph Schuhmann, Romain Beaumont, Richard Vencu, Cade Gordon, Ross Wightman, et al. 2022. LAION-5B: An Open Large-Scale Dataset for Training Next Generation Image-Text Models. In *Proceedings of the 36th International Conference on Neural Information Processing Systems (New Orleans, LA, USA) (NIPS '22)*. Curran Associates Inc., Red Hook, NY, USA, Article 1833, 17 pages.
- [39] Mohammad Shoeybi, Mostofa Patwary, Raul Puri, Patrick LeGresley, Jared Casper, et al. 2020. Megatron-LM: Training Multi-Billion Parameter Language Models Using Model Parallelism. arXiv. arXiv:1909.08053 [cs.CL] <https://arxiv.org/abs/1909.08053>
- [40] Shezheng Song, Xiaopeng Li, Shasha Li, Shan Zhao, Jie Yu, et al. 2025. How to Bridge the Gap between Modalities: Survey on Multimodal Large Language Model. arXiv. arXiv:2311.07594 [cs.CL] <https://arxiv.org/abs/2311.07594>
- [41] HiGHS Team. 2025. HiGHS: Linear Optimization Software. <https://github.com/ERGO-Code/HiGHS>.
- [42] Ye Tian, Zhen Jia, Ziyue Luo, Yida Wang, and Chuan Wu. 2024. DiffusionPipe: Training Large Diffusion Models with Efficient Pipelines. In *Proceedings of Machine Learning and Systems*.
- [43] Colin Unger, Zhihao Jia, Wei Wu, Sina Lin, Mandeep Baines, et al. 2022. Unity: Accelerating DNN Training Through Joint Optimization of Algebraic Transformations and Parallelization. In *16th USENIX Symposium on Operating Systems Design and Implementation (OSDI 22)*.
- [44] Ashish Vaswani, Noam Shazeer, Niki Parmar, Jakob Uszkoreit, Llion Jones, et al. 2017. Attention is All You Need. In *Conference on Neural Information Processing Systems (Long Beach, California, USA) (NIPS'17)*. Curran Associates Inc., Red Hook, NY, USA, 6000–6010.
- [45] Peng Wang, Shuai Bai, Sinan Tan, Shijie Wang, Zhihao Fan, et al. 2024. Qwen2-VL: Enhancing Vision-Language Model's Perception of the World at Any Resolution. arXiv. arXiv:2409.12191 [cs.CV] <https://arxiv.org/abs/2409.12191>
- [46] Yi Wang, Yanan He, Yizhuo Li, Kunchang Li, Jiashuo Yu, et al. 2024. InternVid: A Large-Scale Video-Text Dataset for Multimodal Understanding and Generation. arXiv. arXiv:2307.06942 [cs.CV] <https://arxiv.org/abs/2307.06942>
- [47] Yujie Wang, Shenhan Zhu, Fangcheng Fu, Xupeng Miao, Jie Zhang, et al. 2025. Spindle: Efficient Distributed Training of Multi-Task Large Models via Wavefront Scheduling. In *Proceedings of the 30th ACM International Conference on Architectural Support for Programming Languages and Operating Systems, Volume 2 (Rotterdam, Netherlands) (ASPLOS '25)*. Association for Computing Machinery, New York, NY, USA, 1139–1155. doi:10.1145/3676641.3715992
- [48] Zheng Wang, Anna Cai, Xinfeng Xie, Zaifeng Pan, Yue Guan, et al. 2025. WLB-LLM: Workload-Balanced 4D Parallelism for Large Language Model Training. In *19th USENIX Symposium on Operating Systems Design and Implementation (OSDI 25)*.
- [49] Jun Xu, Tao Mei, Ting Yao, and Yong Rui. 2016. MSR-VTT: A Large Video Description Dataset for Bridging Video and Language. In *2016 IEEE Conference on Computer Vision and Pattern Recognition (CVPR)*. 5288–5296. doi:10.1109/CVPR.2016.571
- [50] An Yang, Baosong Yang, Binyuan Hui, Bo Zheng, Bowen Yu, et al. 2024. Qwen2 Technical Report. arXiv. arXiv:2407.10671 [cs.CL] <https://arxiv.org/abs/2407.10671>
- [51] An Yang, Baosong Yang, Beichen Zhang, Binyuan Hui, Bo Zheng, et al. 2025. Qwen2.5 Technical Report. arXiv. arXiv:2412.15115 [cs.CL] <https://arxiv.org/abs/2412.15115>
- [52] Yujia Zhai, Chengquan Jiang, Leyuan Wang, Xiaoying Jia, Shang Zhang, et al. 2023. ByteTransformer: A High-Performance Transformer Boosted for Variable-Length Inputs. In *2023 IEEE International Parallel and Distributed Processing Symposium (IPDPS)*. IEEE Computer Society, Los Alamitos, CA, USA, 344–355. doi:10.1109/IPDPS54959.2023.00042
- [53] Zili Zhang, Yinmin Zhong, Ranchen Ming, Hanpeng Hu, Jianjian Sun, et al. 2024. DistTrain: Addressing Model and Data Heterogeneity with Disaggregated Training for Multimodal Large Language Models. arXiv. arXiv:2408.04275 [cs.DC] <https://arxiv.org/abs/2408.04275>
- [54] Hairui Zhao, Qi Tian, Hongliang Li, and Zizhong Chen. 2025. FlexPipe: Maximizing Training Efficiency for Transformer-Based Models with Variable-Length Inputs. In *2025 USENIX Annual Technical Conference (USENIX ATC 25)*. USENIX Association, Boston, MA, USA, 143–159.
- [55] Yanli Zhao, Andrew Gu, Rohan Varma, Liang Luo, Chien-Chin Huang, et al. 2023. PyTorch FSDP: Experiences on Scaling Fully Sharded Data Parallel. arXiv. arXiv:2304.11277 [cs.DC] <https://arxiv.org/abs/2304.11277>
- [56] Lianmin Zheng, Zhuohan Li, Hao Zhang, Yonghao Zhuang, Zhifeng Chen, et al. 2022. Alpa: Automating Inter- and Intra-Operator Parallelism for Distributed Deep Learning. In *16th USENIX Symposium on Operating Systems Design and Implementation (OSDI 22)*.
- [57] Yijie Zheng, Bangjun Xiao, Lei Shi, Xiaoyang Li, Faming Wu, et al. 2025. Orchestrate Multimodal Data with Batch Post-Balancing to Accelerate Multimodal Large Language Model Training. arXiv. arXiv:2503.23830 [cs.DC] <https://arxiv.org/abs/2503.23830>
- [58] Wanrong Zhu, Jack Hessel, Anas Awadalla, Samir Yitzhak Gadre, Jesse Dodge, et al. 2023. Multimodal C4: An Open, Billion-Scale Corpus of Images Interleaved with Text. arXiv. arXiv:2304.06939 [cs.CV] <https://arxiv.org/abs/2304.06939>